Oxygen Content and Bias Influence on Amorphous InGaZnO TFT-Based Temperature Sensor Performance

Sungju Choi, Seohyeon Kim, Jungkyu Jang, Jungmok Kim, Dong Myong Kim, *Member, IEEE*, Sung-Jin Choi, Hyun-Sun Mo, Seung Min Lee, and Dae Hwan Kim, *Senior Member, IEEE*

***Abstract*—A temperature (T) sensor based on an amorphous InGaZnO (a-IGZO) thin-film transistor (TFT) is demonstrated and its performance is analyzed quantitatively. The performance analysis includes the influences of the gate-to-source bias (V_{GS}) and oxygen content in IGZO on the mobility (μ), threshold voltage (V_T), and drain-to-source current (I_{DS}) of TFTs. The linearity and sensitivity of the sensor are found to improve with decreasing oxygen content and increasing V_{GS}, because $\partial I_{DS}/\partial T$ is quantitatively dominated by μ and ($V_{GS} - V_T$) rather than by $\partial\mu/\partial T$ and $-\partial V_T/\partial T$. This indicates that the IGZO TFT has great potential as a temperature sensor in terms of immunity in device/process variation. A sensitivity of 125 nA/K with 1.55 K resolution over a temperature range of 303–373 K was successfully demonstrated in low oxygen and V_{GS} = 9 V conditions.**

***Index Terms*—Temperature sensor, oxygen content, IGZO TFT, sensitivity, percolation barrier, activation energy.**

I. Introduction

AMORPHOUS InGaZnO (a-IGZO) is the most popular oxide material because of its good uniformity over large areas, low processing temperature, high mobility (>10 cm^{2}V^{-1}s^{-1}), extremely low off-current ($<10^{-13}$ A), and compatibility with integration on flexible substrates. Flexible processors and programmable circuits based on a-IGZO thin-film transistors (TFTs) have been successfully applied in wearable devices, and these transistors are important building blocks for wearable healthcare and internet-of-things applications [1]. Although few sensors have been successfully integrated with a-IGZO TFT-based flexible circuits [2], the signal-to-noise would be further improved if the sensors themselves are fabricated with a-IGZO material and homogeneously integrated with the flexible circuitry based on a-IGZO

Manuscript received August 3, 2019; revised August 21, 2019; accepted August 21, 2019. Date of publication August 23, 2019; date of current version September 25, 2019. This work was supported by the National Research Foundation of Korea (NRF) through the Ministry of Education, Science and Technology (MEST), Korean Government, under Grant 2016R1A5A1012966, Grant 2017R1A2B4006982, Grant 18ZB1800, and Grant 2016M3A7B4909668. *(Sungju Choi and Seohyeon Kim contributed equally to this work.)* The review of this letter was arranged by Editor A. Chin. *(Corresponding authors: Seung Min Lee; Dae Hwan Kim.)*

The authors are with the School of Electrical Engineering, Kookmin University, Seoul 02707, South Korea (e-mail: smlee27@kookmin.ac.kr; drlife@kookmin.ac.kr).

Color versions of one or more of the figures in this letter are available online at http://ieeexplore.ieee.org.

Digital Object Identifier 10.1109/LED.2019.2937157

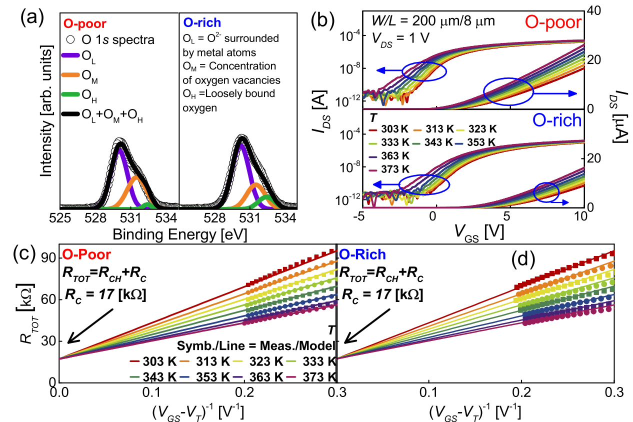

Fig. 1. (a) XPS spectra of O 1s peak upon varying the OFR from Ar: O_2 = 35: 21 (O-poor) to 35: 63 sccm (O-rich). (b) T-dependent transfer characteristics. T-dependent relationships of R_{TOT} with respect to $(V_{GS} - V_T)^{-1}$ in (c) O-poor and (d) O-rich TFT devices. The extracted R_C is found to be independent of T.

TFTs. Therefore, for the systematic design and optimization of a-IGZO-based sensors, their performance needs to be carefully characterized along with variation of the process parameters and bias conditions.

In this study, the influences of oxygen (O) content and gate-to-source bias voltage (V_{GS}) on the performance of a-IGZO TFT-based temperature sensors, including immunity to device-variations, sensitivity, linearity, repeatability, and resolution, are quantitatively analyzed and design guide is discussed.

II. Experimental Procedure

The fabrication procedure for bottom gate IGZO TFTs was described in a previous study [3]. The channel width/length (W/L) is 200/8 μm. In particular, the oxygen content was controlled by varying the oxygen flow rate (OFR) from *O-poor* (Ar: O_2 = 35: 21 sccm) to *O-rich* (35: 63 sccm) conditions when a 50-nm-thick a-IGZO film was DC-sputter-deposited (3 kW) at room temperature (RT).

In Fig. 1(a), X-ray photoelectron spectroscopy (XPS) analysis clearly demonstrates that the amount of oxygen vacancies (V_Os) [O_M] decreases with increasing OFR. This result suggests that the oxygen content is proportional to the trend in the OFR. Temperature (T)-dependencies of the TFT transfer characteristics were measured at the drain-to-source voltage (V_{DS}) = 1 V upon varying T from 303 K to 373 K in 10 K steps [Fig. 1(b)]. Moreover, the TFT contact resistance (R_C) value was extracted by linear extrapolation of

0741-3106 © 2019 IEEE. Personal use is permitted, but republication/redistribution requires IEEE permission. See http://www.ieee.org/publications_standards/publications/rights/index.html for more information.

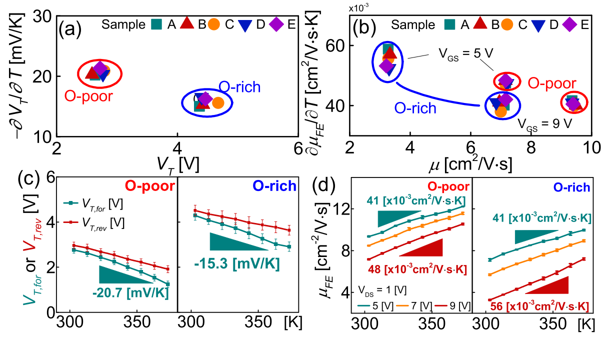

Fig. 2. (a) V_T versus $\partial V_T/\partial T$ and (b) μ_{FE} versus $\partial\mu_{FE}/\partial T$ relationships, which are taken from the RT transfer characteristics of five IGZO TFTs (from A to E). T-dependencies of (c) V_T and (d) μ_{FE}. Here V_T is defined as either $V_{T,for}$ (the V_T taken from the transfer curve varying V_{GS} from -10 V to 10 V) or $V_{T,rev}$ (from 10 V to -10 V). In (a), V_T is shown using $V_{T,for}$. In addition, in (c) and (d), the symbol and error bar indicate the average value (m) and one standard deviation (σ), respectively, taken from five TFT devices.

the total TFT resistance (R_{TOT}) versus $(V_{GS} - V_T)^{-1}$ relationship, with a threshold voltage (V_T) extracted by a linear extrapolation from the transfer characteristics in Fig. 1(b). Figures 1(c) and (d) show that R_C is independent of either the oxygen content or T. Furthermore, the repeatability was confirmed with the observation that during the six T-varying cycles, the T-dependent drain-to-source current (I_{DS}) was well reproduced within an error rate of 5% (not shown). The density of conduction-band (CB) localized states in the subgap energy level E near the CB minimum (E_C), i.e., $g_A(E)$, is widely modeled as:

$$g_A(E) = N_{DA} \times \exp\left(\frac{E - E_C}{kT_{DA}}\right) + N_{TA} \times \exp\left(\frac{E - E_C}{kT_{TA}}\right), \tag{1}$$

where N_{DA}/N_{TA} and kT_{DA}/kT_{TA} are the density of deep/tail acceptor-like traps and the characteristic energy of deep/tail states, respectively. The parameters were extracted to be $N_{DA} = 1.5 \times 10^{17}/2.5 \times 10^{17}$ [cm^{-3}eV^{-1}], $kT_{DA} = 0.8/0.7$ [eV], $N_{TA} = 1.0 \times 10^{18}/1.4 \times 10^{18}$ [cm^{-3}eV^{-1}], and $kT_{TA} = 0.035/0.045$ [eV] for the O-poor/O-rich device by using the unified subthreshold coupling factor technique [4]. The $g_A(E)$ increases with the OFR, because of the increased ion bombardment during the sputtering process [3], especially when the oxygen content is controlled by modulating the OFR.

III. Results and Discussions

A. Device-to-Device Variation

To estimate the immunity of the sensing performance to device-to-device variation, V_T versus $\partial V_T/\partial T$ and the field-effect mobility (μ_{FE}) versus $\partial\mu_{FE}/\partial T$ relationships were assessed from the room temperature (RT) and T-dependent transfer characteristics of five TFTs (from A to E), as shown in Figs. 2(a) and (b). Lower V_T in O-poor TFT originates from higher electron concentration, because V_Os act as donors in IGZO [5]. Additionally, the lower O-content and the large V_{GS} cause μ_{FE} to increase and $\partial\mu_{FE}/\partial T$ to decrease.

The physical origin of the effects of O-content and V_{GS} on μ_{FE} and $\partial\mu_{FE}/\partial T$ can be explained as follows. In amorphous multi-metal oxides, some potential barriers felt by electrons in E_C inherently exist between neighboring ions. These barriers hinder electron transport and lower the mobility (μ) because

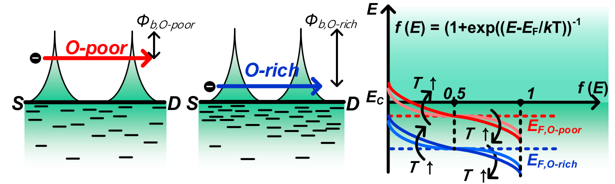

Fig. 3. Schematic of electron conduction via effective CB percolation barrier with a Fermi-Dirac distribution.

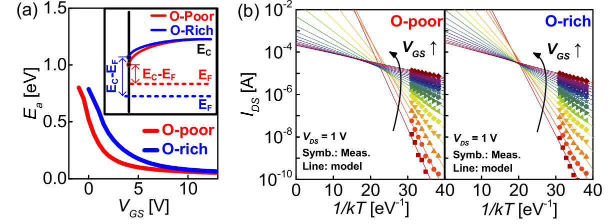

Fig. 4. (a) Relationship of E_a versus V_{GS}. Inset shows the TCAD simulation result. (b) Arrhenius plot of T-dependent I_{DS} versus inverse of thermal energy.

of the different radii of metal ions, which results from the non-uniform overlap of conduction electron orbitals among In-O, Ga-O, and Zn-O bonds (Fig. 3). Thus, this potential barrier in the CB is the main factor determining $\mu_{FE}(V_O, V_{GS})$ and $\partial\mu_{FE}/\partial T(V_O, V_{GS})$. Subsequently, the percolation barrier height (Φ_b in Fig. 3) becomes effectively lower due to the higher Fermi energy level (E_F) in lower O-content or higher V_{GS}, which leads to higher μ_{FE}.

With respect to $\partial\mu_{FE}/\partial T(V_O, V_{GS})$, the activation energy (E_a) follows the Meyer-Neldel (MN) rule, which represents the intrinsic property of a disordered semiconductor. The MN rule has been explained by a trap-limited conduction model [6], a percolation model [6], [7], and a statistical shift in E_F [8], and it has been described by the relationships of $I_{DS} = I_{DS0} \times exp(-E_a/kT)$ and $I_{DS0} = I_{DS00} \times exp(-E_a \times A)$. Based on these relations, E_a can be extracted from the Arrhenius plots [Fig. 4(b)], as seen in Fig. 4(a). E_a was extracted as 0.10/0.176 eV (V_{GS} = 5 V) and 0.066 / 0.089 eV (V_{GS} = 9 V) for the O-poor/O-rich devices [Fig. 4(a)], and it can be optimized by controlling either the bias or the O-content in IGZO.

The E_a of the O-rich device is higher than that of the O-poor device in a broad range of V_{GS}. This means that in O-rich case, more thermal energy is required for electrons to escape from the localized traps than in the O-poor case [inset of Fig. 4(a)]. This $E_a(V_O, V_{GS})$ efficiently explains a larger $\partial\mu_{FE}/\partial T$ in O-rich IGZO. It is also consistent with the trap-limited and percolation conduction models. When the temperature increases, more carriers are thermally activated and released from the subgap trap sites to the CB, followed by higher μ_{FE} of carriers assisted by lower E_a, increasing E_F, and effective lowering of Φ_b. This leads to a positive $\partial\mu_{FE}/\partial T$ [Figs. 2(b) and (d)]. Consistently, the more negative $\partial V_T/\partial T$ in the O-poor device [Figs. 2(a) and (c)] is likewise well explained by lower E_a, followed by stronger T-dependency of I_{DS}.

In Figs. 2(a) and (b), V_T and μ_{FE} have values ranging from 1 to 13. At a specific T, they have the same order of magnitude, while the device-to-device variation of V_T is larger than that of μ_{FE}. The higher the oxygen content in IGZO is, the larger the device-to-device variation of μ_{FE} and the V_{GS}-dependence of the μ_{FE} variation, because the separation

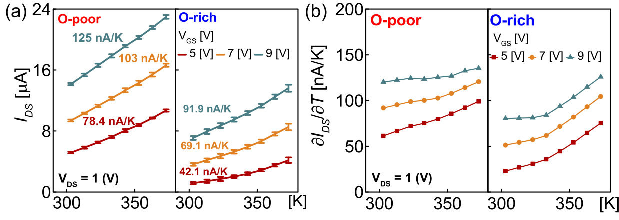

Fig. 5. T-dependencies of (a) I_{DS} and (b) $\partial I_{DS}/\partial T$ with varying O-content and V_{GS}. In (a), the symbol and error bar indicate the average value (m) and one standard deviation (σ) taken from five TFT devices. In (b), the symbols indicate m's of $\partial I_{DS}/\partial T$ taken from five TFT devices.

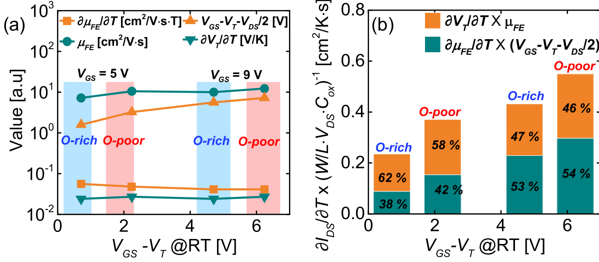

Fig. 6. Effects of $(V_{GS} - V_T)$ and O-content on four terms consisting of (a) $\partial I_{DS}/\partial T$ at RT and (b) $\partial I_{DS}/\partial T$ normalized by $C_{ox} \times (W/L) \times V_{DS}$. The percentages depict the contributions of each term.

between E_C and E_F becomes larger [Fig. 4(a)]. Moreover, higher oxygen content leads to larger V_T device-to-device variation, because of the same reason as larger E_a. Variations of V_T and μ can be further improved by optimization of the fabrication process, which will lead to improved temperature sensor performance. However, the eventual variation of the temperature sensor performance is determined by the distributions of I_{DS} and $\partial I_{DS}/\partial T$ rather than by the variations of V_T, $\partial V_T/\partial T$, μ, and $\partial \mu/\partial T$.

To quantitatively analyze $\partial I_{DS}/\partial T$ more in detail, the T-dependencies of I_{DS} and $\partial I_{DS}/\partial T$ with varying O-content and V_{GS} are shown in Fig. 5 and described in (2) and (3) as follows:

$$I_{DS} = \mu C_{ox} \frac{W}{L} \left[(V_{GS} - V_T) V_{DS} - \frac{1}{2} V_{DS}^2 \right] \quad (2)$$

$$\frac{\partial (I_{DS})}{\partial T} = C_{ox} \frac{W}{L} V_{DS} \left[\frac{\partial \mu}{\partial T} \left(V_{GS} - V_T - \frac{1}{2} V_{DS} \right) - \mu \frac{\partial V_T}{\partial T} \right], \quad (3)$$

where C_{ox} is the gate oxide capacitance per unit area. The four terms consisting of $\partial I_{DS}/\partial T$ in (3), including $\partial \mu/\partial T$, $(V_{GS} - V_T - 0.5 \times V_{DS})$, μ, and $-\partial V_T/\partial T$, are plotted around RT, as shown in Figs. 6(a) and (b). $\partial I_{DS}/\partial T$ is dominated by μ and $(V_{GS} - V_T)$ rather than by $\partial \mu/\partial T$ and $-\partial V_T/\partial T$, because the two former values have a higher order of magnitude than those of the latter two values. Interestingly, even though there are variations of V_T or μ, the robust and significantly uniform performance of the IGZO TFT-based temperature sensor is attainable only if either the O-content or V_{GS} condition is optimized (Fig. 5), because the $\partial I_{DS}/\partial T$ is quantitatively dominated by μ or $(V_{GS} - V_T)$ rather than by $\partial \mu/\partial T$ or $-\partial V_T/\partial T$.

B. Sensitivity

In Fig. 2, $\partial V_T/\partial T$ and $\partial \mu/\partial T$ have negative and positive values, respectively. In addition, $-\partial V_T/\partial T$ has the same order of magnitude as $\partial \mu/\partial T$, and $\partial \mu/\partial T$ is larger than $-\partial V_T/\partial T$. When V_{GS} is lower and/or when the IGZO is O-rich, $\partial \mu/\partial T$ increases significantly. In this case, it is likely that the sensitivity ($= \partial I_{DS}/\partial T$) should be improved by lowering V_{GS} and enhancing O-content in IGZO, however this was not observed. Rather, as the O-content decreases and V_{GS} increases, $\partial I_{DS}/\partial T$ increases (Fig. 5). This is because as mentioned in (3), $\partial I_{DS}/\partial T$ is quantitatively dominated by μ and $(V_{GS} - V_T)$ rather than by $\partial \mu/\partial T$ and $-\partial V_T/\partial T$. In detail, as the oxygen content in IGZO decreases, V_T decreases and μ increases. Moreover, as V_{GS} increases, μ also increases. Therefore, as the O-content decreases in IGZO and as V_{GS} increases, both μ and $(V_{GS} - V_T)$ increase, resulting in higher $\partial I_{DS}/\partial T$ sensitivity. Indeed, the largest $\partial I_{DS}/\partial T$ sensitivity of 125 nA/K was observed in O-poor and $V_{GS} = 9$ V conditions as shown in Fig. 5.

C. Linearity

For good linearity, the $\partial I_{DS}/\partial T$ should remain almost unchanged with varying T. The nonlinear relationship between $\partial I_{DS}/\partial T$ and T would be compromised with the burden of complicated circuits or a high-quality interpolation/sampling scheme. As shown in Fig. 5(b), the linearity improves as V_{GS} increases and/or as the O-content in IGZO is smaller. This can be explained as follows. In (3), the sensitivity is determined by two terms, $\partial \mu/\partial T \times (V_{GS} - V_T - 0.5 \times V_{DS})$ and $-\mu \times \partial V_T/\partial T$. In the second term, i.e., $-\mu \times \partial V_T/\partial T$, the device-to-device variation of μ is smaller than that of V_T. $\partial V_T/\partial T$ is also smaller than $\partial \mu/\partial T$. Therefore, with respect to the T-immunity of $\partial I_{DS}/\partial T$, the second term is weaker than the first. Furthermore, the T-dependence of $-\partial V_T/\partial T$, i.e., $\partial^2 V_T/\partial T^2$, is overcome by $\mu(T)$, and the T-immunity of $\partial I_{DS}/\partial T$ is dominated by $\mu(T)$. Meanwhile, in the first term, i.e., $\partial \mu/\partial T \times (V_{GS} - V_T - 0.5 \times V_{DS})$, the T-immunity of $\partial I_{DS}/\partial T$ is dominated by $(V_{GS} - V_T - 0.5 \times V_{DS})$. Although $\partial \mu/\partial T$ is larger than $-\partial V_T/\partial T$, the T-dependence of $\partial \mu/\partial T$, i.e., $\partial^2 \mu/\partial T^2$, is overcome by $V_{GS} - V_T(T)$. Ultimately, the conditions of lower O-content in IGZO and higher V_{GS} contribute to good linearity.

D. Resolution

From the standpoint of resolution of the temperature sensor (ΔT_{error}), the deviation of I_{DS} (σ_{IDS}) should be considered with the formula: $\Delta T_{error} = (\partial I_{DS}/\partial T)^{-1} \times \sigma_{IDS}$. The ΔT_{error} of 1.55 K is attainable over a temperature range of 303–373 K if the O-poor and $V_{GS} = 9$ V conditions are used. Therefore, the ΔT_{error} can be further reduced via optimization of O-content and V_{GS} conditions.

IV. Conclusion

Influences of the O-content and V_{GS} on the performances of a-IGZO TFT-based temperature sensors, such as immunity on device-variations, sensitivity, linearity, repeatability, and resolution, are quantitatively analyzed, and their design guide is discussed; 1) the lower O-content in IGZO and higher V_{GS} conditions are advantageous from the viewpoints of good linearity and sensitivity, 2) the I_{DS}, which determines the dynamic range, sensing speed, readout circuitry, and operating point, can be controlled and should be optimized in a manner dependent on the application by modulating $C_{ox} \times W/L \times V_{DS}$; 3) in terms of low power consumption, V_{GS} should be as low as possible when satisfying the two conditions specified above.

References

[1] P. Heremans, N. Papadopoulos, A. de Jamblinne de Meux, M. Nag, S. Steudel, M. Rockele, G. Gelinck, A. Tripathi, J. Genoe, and K. Myny, “Flexible metal-oxide thin film transistor circuits for RFID and health patches,” in *IEDM Tech. Dig.*, vol. 4, Dec. 2016, pp. 6.3.1–6.3.4. doi: 10.1109/IEDM.2016.7838360.

[2] K. Takei, “High performance, flexible CMOS circuits and sensors toward wearable healthcare applications,” in *IEDM Tech. Dig.*, Dec. 2016, pp. 6.1.1–6.1.4. doi: 10.1109/IEDM.2016.7838358.

[3] S. Kim, Y. W. Jeon, Y. Kim, D. Kong, H. K. Jung, M.-K. Bae, J.-H. Lee, B. D. Ahn, S. Y. Park, J.-H. Park, J. Park, H.-I. Kwon, D. M. Kim, and D. H. Kim, “Impact of oxygen flow rate on the instability under positive bias stresses in DC-sputtered amorphous InGaZnO thin-film transistors,” *IEEE Electron Device Lett.*, vol. 33, no. 1, pp. 62–64, Jan. 2012. doi: 10.1109/led.2011.2173153.

[4] S. Jun, C. Jo, H. Bae, H. Choi, D. H. Kim, and D. M. Kim, “Unified subthreshold coupling factor technique for surface potential and subgap density-of-states in amorphous thin film transistors,” *IEEE Electron Device Lett.*, vol. 34, no. 5, pp. 641–643, May 2013. doi: 10.1109/LED.2013.2248116.

[5] T. Kamiya, K. Nomura, M. Hirano, and H. Hosono, “Electronic structure of oxygen deficient amorphous oxide semiconductor a-$InGaZnO_{4-x}$: Optical analyses and first-principle calculations,” *Phys. Status Solidi*, vol. 5, no. 9, pp. 3098–3100, Jul. 2008. doi: 10.1002/pssc.200779300.

[6] S. Lee, A. Nathan, J. Robertson, K. Ghaffarzadeh, M. Pepper, S. Jeon, C. Kim, I.-H. Song, U.-I. Chung, and K. Kim, “Temperature dependent electron transport in amorphous oxide semiconductor thin film transistors,” in *IEDM Tech. Dig.*, Dec. 2011, pp. 14.6.1–14.6.4. doi: 10.1109/IEDM.2011.6131554.

[7] K. Nomura, A. Takagi, T. Kamiya, H. Ohta, M. Hirano, and H. Hosono, “Amorphous oxide semiconductors for high-performance flexible thin-film transistors,” *Jpn. J. Appl. Phys.*, vol. 45, no. 5, pp. 4303–4308, Apr. 2006. doi: 10.1143/JJAP.45.4303.

[8] C. Chen, K. Abe, H. Kumomi, and J. Kanicki, “Density of states of a-InGaZnO from temperature-dependent field-effect studies,” *IEEE Trans. Electron Devices*, vol. 56, no. 6, pp. 1177–1183, Jun. 2009. doi: 10.1109/TED.2009.2019157.